

# Conditioning the $\gamma$ spectrometer for activity measurement at very high background\*

YAN Wei-Hua(闫威华)<sup>1</sup> ZHANG Li-Guo(张立国)<sup>2</sup> ZHANG Zhao(张钊)<sup>1</sup> XIAO Zhi-Gang(肖志刚)<sup>1;1)</sup>

<sup>1</sup> Department of Physics, Tsinghua University, Beijing 100084, China

<sup>2</sup> Institute of Nuclear Energy and Technology, Tsinghua University, Beijing 100084, China

**Abstract:** The application of a high purity Germanium (HPGe)  $\gamma$  spectrometer in determining the fuel element burnup in a future reactor is studied. The HPGe detector is exposed by a  $^{60}\text{Co}$  source with varying irradiation rate from  $10 \times 10^3 \text{ s}^{-1}$  to  $150 \times 10^3 \text{ s}^{-1}$  to simulate the input counting rate in real reactor environment. A  $^{137}\text{Cs}$  and a  $^{152}\text{Eu}$  source are positioned at given distances to generate a certain event rate in the detector with the former being proposed as a labeling nuclide to measure the burnup of a fuel element. It is shown that both the energy resolution slightly increasing with the irradiation rate and the passthrough rate at high irradiation level match the requirement of the real application. The influence of the background is studied in the different parameter sets used in the specially developed procedure of background subtraction. It is demonstrated that with the typical input irradiation rate and  $^{137}\text{Cs}$  intensity relevant to a deep burnup situation, the precision of the  $^{137}\text{Cs}$  counting rate in the current experiment is consistently below 2.8%, indicating a promising feasibility of utilizing an HPGe detector in the burnup measurement in future bed-like reactors.

**Key words:** fuel element burnup,  $\gamma$  activity, HPGe,  $\gamma$  spectrometer

**PACS:** 29.30.Kv, 28.41.Bm, 28.50.Dr      **DOI:** 10.1088/1674-1137/36/11/008

## 1 Introduction

Fuel balls undergo a multipass cycle in modular pebble bed reactors (MPBR). Because of the serious inaccuracy of the computational method, which is conventional for performing the in-core fuel management in existing water reactors, a non-destructive determination of the burnup is desired in order to provide the distributed controlling system with an on-line circulation/discharge judgement on a pebble-by-pebble basis in some bed-like reactors [1, 2]. Gamma ray spectrometry has been proposed as an effective non-destructive method to determine the burnup [3–7] as well as the spatial irradiation distribution [8, 9] by measuring the activity (activity ratio) of given monitor nuclide(s). Among all kinds of fission products,  $^{137}\text{Cs}$  has been proposed to be one of the most effective burnup indicators for its long lifetime and clear correspondence to the burnup of the fuel pebble with significant resistance to the power history

[10, 11]. Nevertheless, the fission of the fissile materials in MBPR produces various radioactive nuclides that emit an amount of  $\gamma$  peaks over the whole spectrum, and hence, as shown by various simulation results [1, 12–14] and some testing results, the  $^{137}\text{Cs}$  full energy peak is likely to be obscured by the neighboring  $\gamma$  rays in a typically short cooling time. For instance, in almost all stages of the burnup, a peak of 658 keV from  $^{97}\text{Nb}$  is presented. Thus, in order to identify the  $\gamma$  peak from the  $^{137}\text{Cs}$  662 keV, a  $\gamma$  spectrometer with energy resolution of better than 2 keV is highly desirable. In this regard, the high purity germanium (HPGe)  $\gamma$  detector has been widely proposed as a non-destructive method for the determination of fuel pebble burnup.

Another feature of the fuel element with a certain burnup in future reactors is the high  $\gamma$  radioactivity. According to the prediction, the radiation exposure of the HPGe detector varies from  $10 \times 10^3 \text{ s}^{-1}$  to more than  $150 \times 10^3 \text{ s}^{-1}$ , depending on the shielding

Received 24 February 2012

\* Supported by National Science and Technology Major Project (ZX06901), National Natural Science Foundation of China (10975083) and Tsinghua University Initiative Scientific Research Program

1) E-mail: xiaozg@tsinghua.edu.cn

©2012 Chinese Physical Society and the Institute of High Energy Physics of the Chinese Academy of Sciences and the Institute of Modern Physics of the Chinese Academy of Sciences and IOP Publishing Ltd

condition, the geometric collimation, and the cooling time. In the design of the spectrometer, although the dead time of the spectrometer can be lowered by decreasing the irradiation level through a strict geometrical collimator, the net count rate of the labeling  $^{137}\text{Cs}$  is also suppressed and a larger statistical error is expected. Therefore for the MPBR under design, it is of extreme importance to optimize the working parameters, including the shaping time, geometrical collimation, and shielding, in order to determine the activity with a minimized experimental error limit within the typical real time (tens of seconds) after very short cooling time (typically tens of hours).

In this paper, we present the main results from the experimental conditioning of an HPGe  $\gamma$  spectrometer. The passthrough curves at different shaping times and flattop are measured. For the appropriately chosen shaping time, the peak resolution is measured with various radiation background levels. Furthermore, the precision of measuring the net counts of a  $^{137}\text{Cs}$  source is studied in detail by varying the real time, the net rate of the nuclide of interest (NOI) and the radiation background level. In Section 2, the experimental setup and conditions are described. Section 3 presents the main results and Section 4 is the summary.

## 2 The experimental setup

The whole spectrometer consists of an HPGe  $\gamma$

detector, an electrical cooling device (X-Cooler II) and suitable fast electronics (DSPEC+) from ORTEC. The cylindrical HPGe crystal is 43 mm in height and 62.6 mm in diameter, with a  $\phi 10.8 \text{ mm} \times 30 \text{ mm}$  hollow copper electrical pole fed in the axial center. The efficiency of the HPGe detector for  $^{60}\text{Co}$   $\gamma$  rays is about 30% at the working high voltage +2300 V. The preamplifier adopts the light feed-back technique to reduce the pile-up effect at high incident rate.

Three  $\gamma$  sources are used in the experiment. A  $^{60}\text{Co}$  is applied to simulate the irradiation background from 10 to  $150 \times 10^3 \text{ s}^{-1}$  (dubbed from CO1 to CO15 in the text) by varying its distance to the detector. The intense incident counting rate is controlled by the  $^{60}\text{Co}$  source throughout the test unless specially specified. A  $^{137}\text{Cs}$  is placed at two positions in the vicinity of the detector to generate about 30 (CS1) or 120 (CS2)  $\text{s}^{-1}$  counting rate in the detector to mimic the counting rate of a low and a high burnup element, respectively. Correspondingly, a  $^{152}\text{Eu}$  source is also introduced to investigate the performance of the spectrometer varying with the  $\gamma$  energy. At each geometrical configuration, the measurement is done over 2 settings of the shaping time and the flattop (SHP1 and SHP2) of the main amplifier for 1 or 10 groups, with 5 files in each group. In total 2904 files are acquired. With these measurements it is possible to study the repeatability and the statistic fluctuation of multi observables. Table 1 summarizes the experimental conditions of the multi source experiment.

Table 1. Conditions in the multi source experiment.

subscript	shaping time $\tau_s$ and flattop $\tau_f/\mu\text{s}$		$^{137}\text{Cs}$ intensity $n_{\text{Cs}}/\text{s}^{-1}$ and real time $T_r/\text{s}$		$^{60}\text{Co}$ irradiation rate $n_{\text{Co}} (\times 10^3 \text{ s}^{-1})$		
	SHP1	SHP2	CS1	CS2	CO1	...	CO15
	parameter	$\tau_s = 0.8$	$\tau_s = 1.2$	$n_{\text{Cs}} = 30$	$n_{\text{Cs}} = 130$	$n_{\text{Co}} = 10$	...
setting	$\tau_f = 0.8$	$\tau_f = 0.6$	$T_r = 10$	$T_r = 25$			

## 3 Results and discussions

### 3.1 Passthrough and energy resolution

Figure 1 presents the passthrough curves measured with SHP1 and SHP2. The abscissa depicts the incident  $\gamma$  counting rate characterizing the radiation background level exposed on the detector. The low threshold is 0.3 keV. It is shown that at low radiation level, the passthrough rate increases linearly with the input rate. At about  $100 \times 10^3 \text{ s}^{-1}$ , however, the passthrough starts to deviate with differ-

ent shaping times and undergoes a plateau up to an incident rate of about  $200 \times 10^3 \text{ s}^{-1}$ . Above  $200 \times 10^3 \text{ s}^{-1}$ , the passthrough starts to decrease with the input counting rate due to the rapidly increasing dead time. Unlike the situation with a low input rate, where the passthrough shows an insignificant dependence on the shaping time, the maximum passthrough on the plateau decreases with increasing the shaping time and flattop, as shown in the figure. Quantitatively the passthrough is  $10 \times 10^3 \text{ s}^{-1}$  higher with SHP1 than that with SHP2. In the real application, the amplifier parameters and the geometrical collimation are designed so that the system is running on the

passthrough plateau to acquire the highest statistics while keeping adequate energy resolution since the  $\gamma$  energy peaks in the proximity of the  $^{137}\text{Cs}$  indicator are enriched. As shown later, one can not switch the shaping time down to very small value for the rapidly degraded energy resolution.

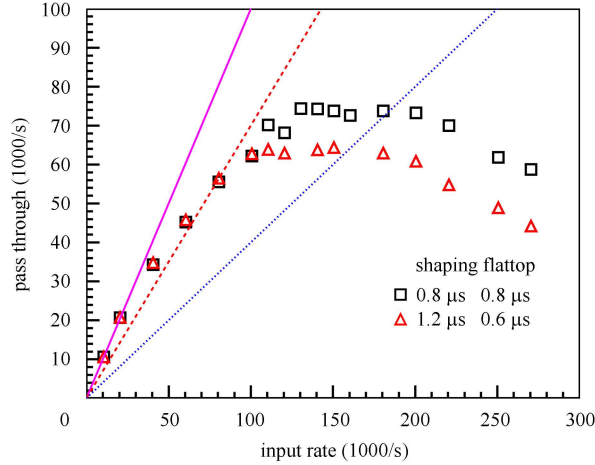


Fig. 1. (color online) Passthrough rate as a function of incident counting rate with SHP1 and SHP2. The solid, dashed and dotted lines represent certain dead times of 0%, 30% and 60%, respectively.

Figure 2 depicts the dependence of the FWHM on the shaping time for  $^{137}\text{Cs}$  and  $^{60}\text{Co}$  peaks. With increasing the shaping time, the FWHM of the full energy peaks decreases rapidly below about 4  $\mu\text{s}$  and then saturates at 1.3 keV and 1.8 keV for  $^{137}\text{Cs}$  and  $^{60}\text{Co}$  full energy peaks, respectively. A shaping time of larger than 0.8  $\mu\text{s}$  is preferred with respect to the required resolution of 1.8 keV for  $^{137}\text{Cs}$ . But because of the high expectation of passthrough, optimization is required. In this paper, only the relevant results with SHP1 and SHP2 are presented since these two conditions meet the requirements of the design for  $\gamma$  spectrometry for the future real application.

The energy dependence of the FWHM is plotted in Fig. 3 at two typical radiation background levels 30 and  $100 \times 10^3 \text{ s}^{-1}$ . The data are fitted with a formulae of  $a\sqrt{E_\gamma + b}$  as shown by the dashed curves. Although on average the data points follow the curves well at both irradiation rates, significant fluctuation of the data points is visible. This is attributed to the relative intensities at different energies of the  $^{152}\text{Eu}$  peaks. The full energy peaks with lower intensities, for instance, at  $E_\gamma = 411$  or 1090 keV, suffer more from the background level induced by the Compton plateau of the intense  $^{60}\text{Co}$  source. And equivalently, the FWHMs become smaller if the incident rate is lowered to  $30 \times 10^3 \text{ s}^{-1}$  as the Compton

background decreases. As expected, the FWHMs of the two  $^{60}\text{Co}$  peaks at 1173 and 1332 keV are not changed by the radiation rate.

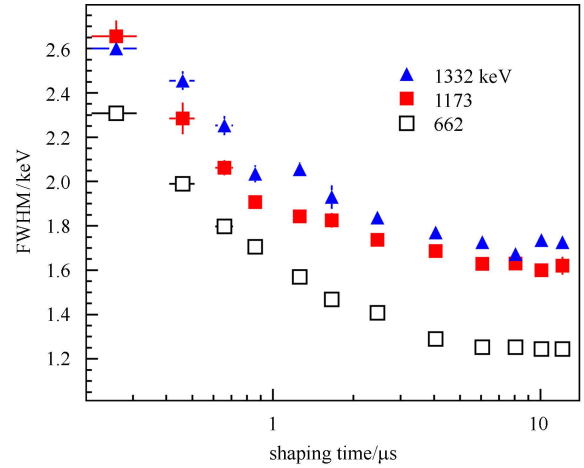


Fig. 2. (color online) FWHM of the full energy peaks as a function of shaping time for the  $^{137}\text{Cs}$  peak (662 keV) and the  $^{60}\text{Co}$  peaks (1173 and 1332 keV).

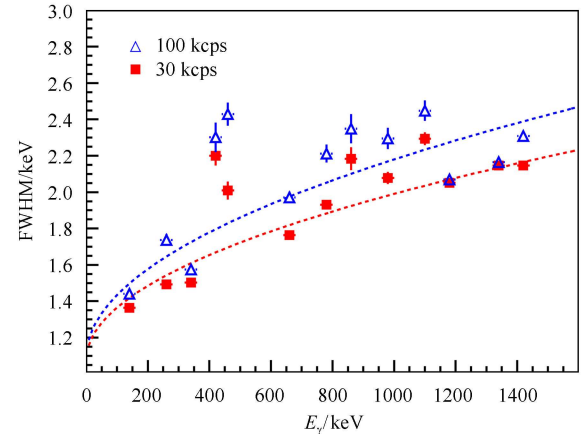


Fig. 3. (color online) FWHM of the full energy peaks as a function of peak energy at different input rates.

Figure 4 presents the FWHM of the  $^{137}\text{Cs}$  full energy peak as a function of incident counting rate at different shaping time configuration SHP1 and SHP2, respectively. Specially, the irradiation rate corresponding to the left panel is controlled by moving the  $^{137}\text{Cs}$  itself. In this case the FWHM keeps constant with the input counting rate. However, in the test where the input counting rate is controlled by moving the  $^{60}\text{Co}$  while the  $^{137}\text{Cs}$  position is fixed, the FWHM exhibits an increasing trend with the input counting rate. At typical input rate of  $30 \times 10^3 \text{ s}^{-1}$  corresponding to deep burnup, the FWHM of the  $^{137}\text{Cs}$  full energy peak is below 1.8 keV. The energy resolution

of the  $^{137}\text{Cs}$  peak is degraded by less than 20% at  $150 \times 10^3 \text{ s}^{-1}$  input rate.

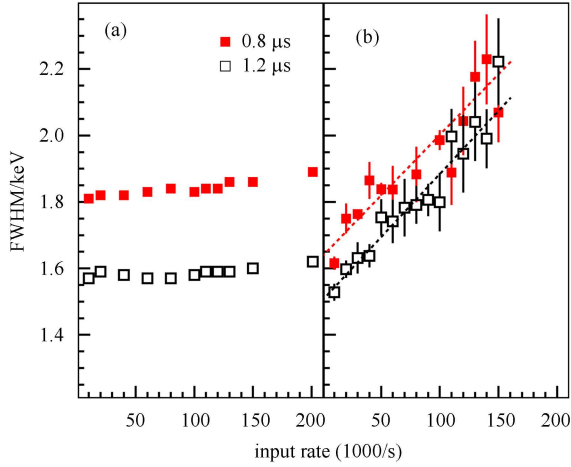


Fig. 4. (color online) FWHM of the full energy peak of  $^{137}\text{Cs}$  as a function of input counting rate at different shaping times for the situations where the incident counting rate is controlled by  $^{137}\text{Cs}$  itself (a) and by the  $^{60}\text{Co}$  source (b).

### 3.2 Precision of the net counts of the NOI

The relationship between the activity of the source  $A$  and the net counting rate of the full energy peak  $n$  recorded by the detector is written as

$$n = A\Gamma\varepsilon, \quad (1)$$

where  $\varepsilon$  is the full energy detection efficiency and  $\Gamma$  is the absolute strength of the peak.  $n$  is obtained by subtracting the background  $B$  from the total counting  $T$  in the range of interest (ROI) corresponding to the full energy peak range via

$$n = \frac{N}{t} = \frac{T - B}{t}, \quad (2)$$

where  $N$  is the net counts recorded in the live time  $t$  of measurement. The standard deviation of the net count  $\sigma_N$  is written as

$$\sigma_N = \sqrt{(\sigma_T)^2 + (\sigma_B)^2} = \sqrt{N + 2B}. \quad (3)$$

In real application, the total background  $B$  is derived by extrapolating the integrated counts  $B_w$  in two predefined windows (with  $CH_b$  channels for each) at the board to the whole ROI (with  $2CH_{hr}$  channels in total) via

$$B = B_w \frac{CH_{hr}}{CH_b}. \quad (4)$$

It is found in the analysis that the net counting rate depends slightly on the range of ROI for the same spectrum. In order to minimize the fluctuation

caused by the change of ROI range, we fix the number of channels of the ROI for each given energy peak at a certain shaping time. Fig. 5 shows the sketch of the procedure of the background subtraction. On both sides of the ROI, each of which is  $CH_{hr}$  to the center of the peak, a fixed window with  $CH_b$  channels at the broad is selected to derive the background by a linear fitting to the data points in these two windows (the green shadowed area). The net peak (the cross symbols) is consequently obtained by subtracting the fitting background (the dashed line) from the total spectrum (the solid histogram). The net area of the peak is then obtained by fitting the net peak with a Gaussian function (the solid curve).

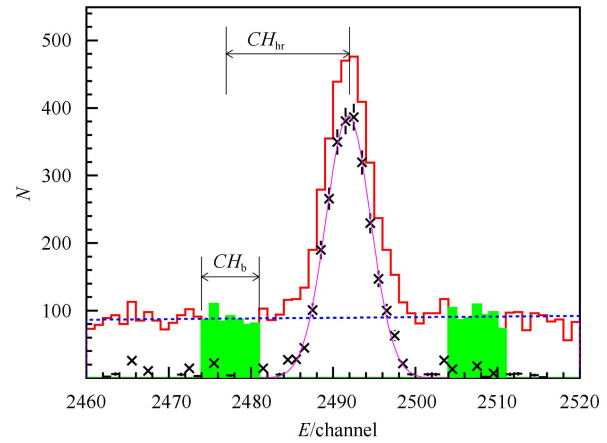


Fig. 5. (color online) Procedure of the background subtraction. The histogram shows the original measured  $\gamma$  spectrum, and the green shadowing area depicts the windows used to fit the background with  $CH_b$  channels for each. The distance between each broad of the ROI to the peak is denoted as  $CH_{hr}$ . The cross symbols represent the net peak after subtracting the fitted background denoted with the dashed line, and the pink curve is a Gaussian fit to the net peak.

Writing the averaged count of the background in a single channel as  $\hat{b}$  for a given radiation background level, from Formulae (3), one then gets the uncertainty of net area

$$\begin{aligned} \sigma_N &= \sqrt{T + \sigma_{B_w}^2 \frac{CH_{hr}^2}{CH_b^2}} = \sqrt{N + B_w \frac{CH_{hr}}{CH_b} + B_w \frac{CH_{hr}^2}{CH_b^2}} \\ &= \sqrt{N + \hat{b}CH_{hr}(1 + CH_{hr}/CH_b)}. \end{aligned} \quad (5)$$

It is shown that the uncertainty of the net area or net rate depends on the background level  $\hat{b}$  as well as the net area  $N$ . Under a given radiation condition, the contribution of the background to  $\sigma_N$  de-

increases with the width of the background window because the fluctuation of the background level, shown with the dashed line in Fig. 5, is weakened by averaging on more channels, as indicated by Formulae (5). Fig. 6 presents the distribution of the background (the left panels) and the net area (the right panels) of  $^{137}\text{Cs}$  peak at different background window width  $CH_b$  for CS1 at about  $30 \times 10^3 \text{ s}^{-1}$  incident counting rate. With  $CH_b$  tuning from 1 to 9, the distributions of the net counts and the background become narrower, indicating a decreasing standard deviation with  $CH_b$ .

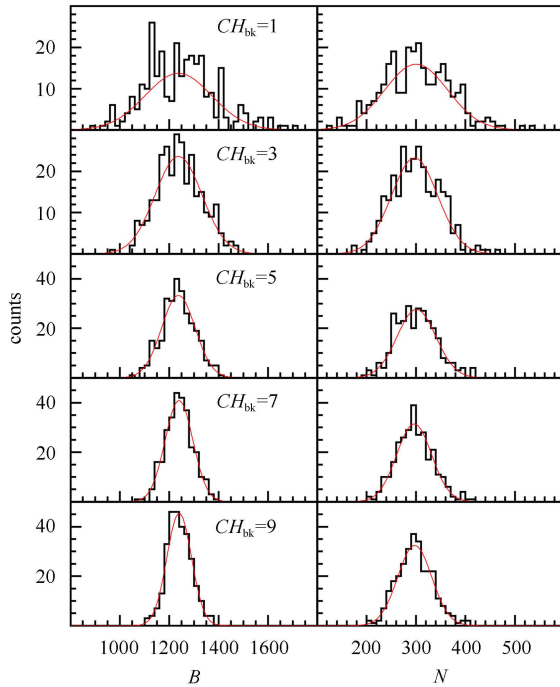


Fig. 6. (color online) Distributions of the background  $B$  (left) and the net counts of  $^{137}\text{Cs}$  peak  $N$  with a different number of channels  $CH_b$  of the background window (see Fig. 5) used to subtract the background

Figure 7 presents quantitatively the relative standard deviation of the background  $\sigma_B/B$  (upper) and of the net area  $\sigma_N/N$  (lower) of  $^{137}\text{Cs}$  peak as a function of  $CH_b$  for CS1 and CS2 at 30, 50 and  $100 \times 10^3 \text{ s}^{-1}$  incident counting rate, respectively. The curves are the fitting with formulae  $\sqrt{c_1 + c_2/N_b}$  with  $c_1$  and  $c_2$  being two fitting parameters. The relative standard deviation of the background is higher at lower irradiation rate while the one of the net area decreases with lowering the radiation background level. The effect of counting time is also clear by comparing the group of CS1 and CS2. With longer measuring time (CS2), both the background and the net area exhibit less uncertainty. At the typical radiation level

of  $30 \times 10^3 \text{ s}^{-1}$  incident rate for the deep burnup fuel element with a  $^{137}\text{Cs}$  counting rate at about  $130 \text{ s}^{-1}$ , the precision of the net rate is better than 3%.

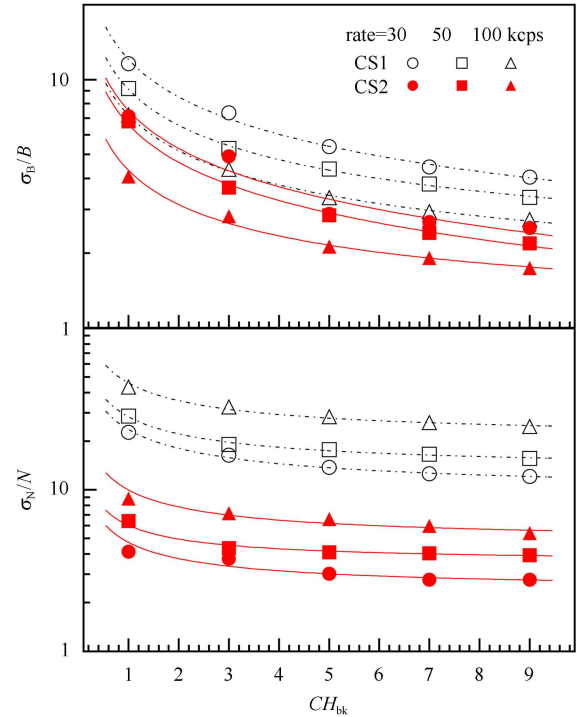


Fig. 7. (color online) The relative standard deviation of the background  $B$  (left) and of total counts  $N$  (and of the net rate of  $^{137}\text{Cs}$  peak  $n$ ) as a function of  $CH_b$  for CS1 and CS2 at different input counting rates.

Figure 8 shows the relative standard deviation profile of the net area of  $^{137}\text{Cs}$  peak as a function of  $^{60}\text{Co}$  irradiation rate for CS1 and CS2, respectively. The symbols are calculated via Formulae (3) with the total area  $T$  and the background  $B$ . The curves, on the other hand, are derived from the corresponding root mean square (RMS) of the net area distributions, as shown exemplarily in the right columns of Fig. 6 at the corresponding radiation level by  $RMS/N$ . It is shown that the curves follow the symbols well with few exceptions where the measurements are repeated less than 5 times. It is shown that the uncertainty of  $N$  increases almost linearly with the radiation background level, showing similar trends for CS1 and CS2. For the CS2 group, for which the  $^{137}\text{Cs}$  source is closer to the detector and the real time is longer, the uncertainty is much smaller.

More investigations including the behavior of  $^{152}\text{Eu}$  peaks in the same measurements reveal more information about the influence of the background level. Fig. 9 shows the correlation between the relative standard deviation for all energy peaks below  $^{60}\text{Co}$  1173 keV as a function of the ratio of the net

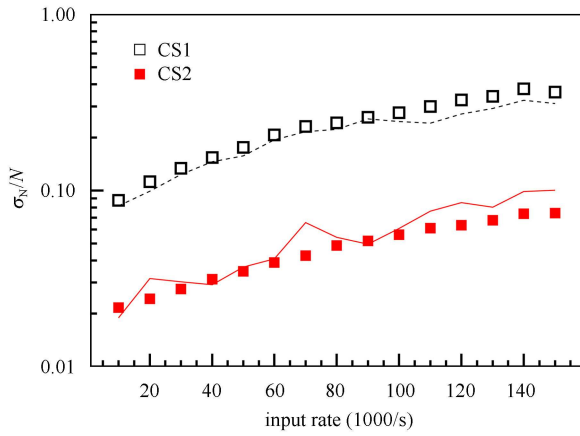


Fig. 8. (color online) Relative uncertainty of the net area as a function of  $^{60}\text{Co}$  irradiation rate for CS1 and CS2. The curves denote the relative standard deviation of the net area distributions, and the symbols are calculated from Formulae (3).

rate and the irradiation rate. Again, the relative uncertainty is calculated via Formulae (4). The pink area corresponds to the CS1 group and the red area to the CS2 group. It is clear that by increasing the measurement time and moving the source closer to the detector, the overall uncertainties are reduced. Since the background level induced by  $^{60}\text{Co}$  varies with the energy and the net rate differs among the  $^{152}\text{Eu}$  peaks, the uncertainty exhibits a significant broadening at a given scaled net rate  $n/I$ . The open triangles and the open squares with quadratic fitting (the dashed curves) present the evolution of the uncertainty of the  $^{137}\text{Cs}$  peak for CS1 and CS2, respectively. From this curve we can estimate the precision of measuring the  $^{137}\text{Cs}$  net rate if the ratio of the net counting rate and radiation background level are roughly known. By

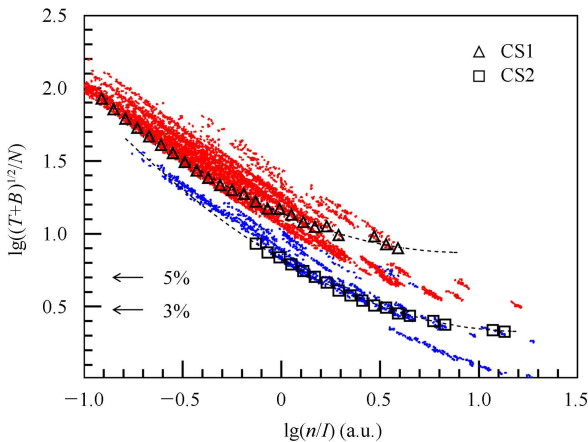


Fig. 9. (color online) Correlation between the relative uncertainty of the net rate and the net rate scaled with the irradiation rates.

neglecting the detailed distribution of the background sources, a precision of 2.8% is again estimated for the deep burnup element in 25-second measurement in the MPBR application under design.

Figure 10 further shows the profile of the measured net counting rate of  $^{137}\text{Cs}$  as a function of the input counting rate for CS1 and CS2. It is shown that below  $100 \times 10^3 \text{ s}^{-1}$  input rate, the net rate keeps constant, revealing a reliable extraction of the net counting rate of the EOI  $^{137}\text{Cs}$ . Again for CS2, corresponding to a deep burnup element in our design, the standard variance of the averaged net rate is within 3%.

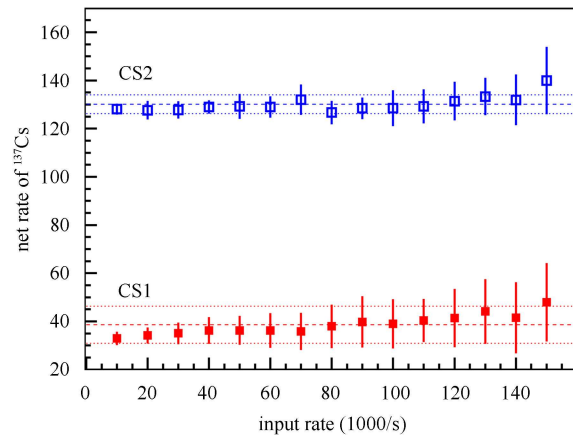


Fig. 10. (color online) The net rate of the  $^{137}\text{Cs}$  measured at different  $^{60}\text{Co}$  irradiation rate for CS1 and CS2. The error bars denote the standard deviation of the net rate distribution in the repeated measurements.

## 4 Summary

In summary, we have studied experimentally the feasibility of utilizing an HPGe detector in the determination of the fuel element burnup in a future bed-like reactor. In the multi source measurement, the passthrough curves are measured by varying the shaping and flattop time of the spectrometer. The plateau of the passthrough rate covers the radiation background level from  $100$  to  $200 \times 10^3 \text{ s}^{-1}$  with adequate energy resolution and allows the implementation of activity measurement of the burnup indicator  $^{137}\text{Cs}$  within a half minute. The energy resolution, reflected by the FWHM of the full energy peak of  $^{137}\text{Cs}$  in this measurement, allows us to identify the peak of  $^{137}\text{Cs}$  with its various neighboring  $\gamma$  rays despite a slight degradation of 20% at very high background

level. The precision ( $1\sigma$ ) of the net counting rate of the EOI  $^{137}\text{Cs}$  under various conditions is studied. It is demonstrated that the subtraction of the background contributes significantly to the total precision of the net area of  $^{137}\text{Cs}$  peak. By fine tuning the background window and fixing the range of interest, the precision ( $1\sigma$ ) is optimized to 2.8% with the typical incident radiation rate and  $^{137}\text{Cs}$  intensity that

is relevant to the deep burnup situation in the future application. It is worth mentioning that because the background composition is much more complicated in a real reactor application than the experimental conditions presented here, a certain deterioration of the precision is expected and demands a detailed simulation (via MCNP or Geant4 for instance) of the real background irradiation.

---

## References

- 1 Hawari A I, CHEN J. IEEE Transactions on Nuclear Science, V, 2002, **49**(3): 1249
- 2 SU B, ZHAO Z, CHEN J, Ayman I. Hawari, Prog. Nucl. Ener., 2006, **48**: 686
- 3 Matsson I. SKI Report, 1995, **95**: 46
- 4 Matsson I, Grapengiessen B. Appl. Radiat. Isot., 1997, **48**(10–12): 1289–1298
- 5 Terremoto L A A, Zeituni C A et al. Nucl. Instrum. Methods A, 2000, **450**: 495
- 6 Ansari S A, Asif M et al. Annals of Nuclear Energy, 2007, **34**: 641
- 7 Willman C, Hakansson A et al. Annals of Nuclear Energy, 2006, **33**: 427
- 8 Khan R, Karimzadeh S, Böck H. Nuclear Engineering and Design, 2010, **240**: 1043
- 9 Maturra S, Tsuruta H et al. Nucl. Sci. Tech., 1975, **12**: 24
- 10 ZHANG L G, LI T S et al. Nuclear Power Engineering, 2008, **29**: 018 (in Chinese)
- 11 Freis D, Nasyrow R, Toscano E H. 3<sup>rd</sup> International Topical Meeting on High Temperature Reactor Technology. South Africa: B00000212, 2006
- 12 Hawari A I, CHEN J. IEEE Transactions on Nuclear Science, 2005, **52**(5): 1659
- 13 CHEN J, Hawari A I, ZHAO Z, SU B. Nucl. Instrum. Methods A, 2003, **505**: 393
- 14 ZHANG L G, SHANG R C. Nuclear Power Engineering, 2009, **30**: 043 (in Chinese)